Evidence of frost-cracking inferred from acoustic emissions in a high-alpine rock-wall

David Amitrano, Stephan Gruber, Lucas Girard

Evidence of frost-cracking inferred from acoustic emissions in a high-alpine rock-wall

D. Amitrano[a], S. Gruber[b], L. Girard[a,b]

[a] *ISTerre, CNRS - Université Joseph Fourier, Grenoble, France.*
[b] *Glaciology, Geomorphodynamics & Geochronology, Dep. of Geography, University of Zurich, Switzerland.*

Abstract

Ice formation within rock is known to be an important driver of near-surface frost weathering as well as of rock damage at the depth of several meters, which may play a crucial role for the slow preconditioning of rock fall in steep permafrost areas. This letter reports results from an experiment where acoustic emission monitoring was used to investigate rock damage in a high-alpine rock-wall induced by natural thermal cycling and freezing/thawing. The analysis of the large catalog of events obtained shows (i) robust power-law distributions in the time and energy domains, a footprint of rock micro-fracturing activity induced by stresses arising from thermal variations and associated freezing/thawing of rock; (ii) an increase in AE activity under sub-zero rock-temperatures, suggesting the importance of freezing-induced stresses. AE activity further increases in locations of the rock-wall that are prone to receiving melt water. These results suggest that the framework of further modeling studies (theoretical and numerical) should include damage, elastic interaction and poro-mechanics in order to describe freezing-related stresses.

Keywords: frost-cracking, acoustic emission, mechanical weathering, scaling properties

1. Introduction

The formation of ice within rock is likely to be an important driver of near-surface frost weathering (Hallet et al., 1991) and rock damage at the depth of

several meters (Murton et al., 2006), and in steep terrain, this process may be crucial for the slow preconditioning of rock fall from warming permafrost areas (Gruber and Haeberli, 2007). However, the transfer of corresponding theoretical insight and laboratory evidence to natural conditions characterized by strong spatial and temporal heterogeneity of the rock properties (e.g. fracture state, water content, thermal and hydraulic conductivity) and thermal conditions is nontrivial. To examine rock fracture in natural conditions, we performed a pilot experiment, monitoring acoustic emissions (AE) in a high-altitude rock-face during a four days period. In such conditions, the mechanical loading of rock results from the combination of a constant gravity load and fluctuating loads related to (i) thermal stresses, arising from the gradient of the temperature field, (ii) pressure variations in rock pores and cracks, due to water or to ice formation and (iii) short-term external loading such as earthquakes. While large thermal stresses can only occur close to the rock surface, ice formation in pores, cracks and fractures can potentially generate large stresses at greater depths, as suggested by theoretical and lab studies. Reporting a preliminary analysis of the microseismic activity monitored at a high alpine ridge, Amitrano et al. (2010) recently stressed the importance of ice formation in fractures as they observed micro-seismic activity corresponding with particular trends of the temperature that could enhance ice formation. But the lack of details in the spatial and temporal distribution of the seismic events precluded the full understanding of the relationship between temperature evolution and related ice formation at small spatial scale and the triggering of seismic events.

The mechanical loading of rocks involves local inelastic processes that produce elastic wave propagation so called acoustic emission (AE) at small scales and micro-seismicity (MS) at larger scales. Beside the common physical origin of the elastic wave emission, essentially induced by the propagation or shearing of cracks, these two terms denote differences in the frequency content of the recorded signals corresponding to sources of different size (see Hardy (2003) for a full presentation). MS relates to the range 1-10^3 Hz whereas AE relates to the range 10^4-10^6 Hz. The corresponding source size is 1-10^3 m for MS and

10^{-3}-10^{-1} m for AE. The material attenuation, that increases with frequency, precludes the detection of AE after approximatively 1 m of wave propagation, whereas MS can be detected at larger distances (up to km).

Measuring AE or MS activity therefore provides a powerful technique to monitor the evolution damage at different scales. Due to their wide frequency range, the simultaneous recording of AE and MS currently is technically not possible. The AE has been extensively used as a tool at the laboratory rock sample scale [e.g. Lockner (1993)] whereas MS has been mostly used at larger scales in order to study seismicity and rockburst in mines, tunnels or quarries (Hardy, 2003). In all these cases, AE/MS are considered to be an indicator of inelastic behavior that can be related to damage increase or to shearing of existing fractures (Cox and Meredith, 1993; Lockner, 1993). Several recent studies report MS monitoring of slope instability (Amitrano et al., 2010; Gaffet et al., 2010). The originality of our study is to apply high frequency AE monitoring, a technique traditionally used in laboratory experiments, to investigate rock damage during freezing, in field conditions. The main advantage of using high frequency monitoring is the sensitivity to emissions of relatively small energies. This allows us to obtain a large catalog of events within a short monitoring period, which is crucial to perform statistical analyses. At such high frequencies, acoustic signals are attenuated within about a meter, which determines the spatial scale of our study. This is an advantage as most of the acoustic activity related to freezing can be expected to occur within a meter from the surface. This technique finally offers a high temporal resolution, as event rates up to 10^3 per second can be detected.

Fracturing dynamics during mechanical loading, usually displays scaling properties in the domains of size, space and time (Alava et al., 2006; Sethna et al., 2001). In the domain of size (magnitude) for example, the seismic events induced by damage processes display a power-law (PL) distribution, $N(s) \sim s^{-b}$, where s is an estimate of the event size (e.g. the maximum amplitude of the AE signal or its energy), $N(s)$ is the probability distribution function (PDF) and b is a constant. This distribution is equivalent to the well-known Gutenberg-

Richter relationship observed for earthquakes (Gutenberg and Richter, 1954). Scaling properties in space and time of the events have also been reported, characterizing their spatial and temporal clustering. The emergence of these scaling properties is considered to be a universal feature of the damage dynamics in heterogeneous media (Alava et al., 2006) as it is observed in a very robust manner for various loading conditions, various materials and scales ranging from the micrometer (microcracks) to thousands of kilometers (the Earth's-crust or the sea ice cover). In this letter we report an original in-situ experiment of AE monitoring in high altitude thermal conditions. We show that AE activity resulting from natural thermal cycling and induced freezing/thawing shows similar scaling properties, suggesting that the local stress fluctuations encountered are high enough to induce micro-fracturing.

2. Measurement site and instrumental setting

The measurement site is a south-facing cliff of granitic gneiss (Wegmann and Keusen, 1998) that is situated at an elevation of 3500 m a.s.l. in the Swiss Alps. The local mean annual air temperature is about -7.3° C (1961–1990), whereas mean annual rock temperatures near the surface are between -2 and -3° C in this south face (Hasler et al., 2011). The site is directly next to the high-altitude research station Jungfraujoch and thus can be measured with standard AE equipment housed inside a heated building.

A six-channel high-frequency acquisition board (Mistras, Euro Physical Acoustic) with 16-bit resolution and 10 V maximum amplitude was used. The AE piezo-electrical sensors (EPA R6I) had an operating frequency range of 10–150 kHz with a peak sensitivity at 60 kHz. They included a pre-amplifier of 40 dB and were connected with 20 meters coaxial cables. The system was continuously sampling with a frequency of 1 MHz and basic signal characteristics such as time, amplitude, energy, duration, spectral content were calculated in real time for events over 35 dB amplitude. The maximum noise amplitude has been measured to be near 1 mV (30 dB), indicating that recorded events were

not induced by noise fluctuations. Full waveforms of 2 ms including a pre-trigger of 0.4 ms were recorded for events over 40 dB (4 mV). Using an ultrasonic coupling gel (Sofranel), sensors were pressed on a steel plate with rubber bands. We verified in the lab that the coupling gel behaves similarly for various temperature and do not generate AE when freezing (Weber et al., 2012). The steel plates were screwed onto extension bolts (10 mm diameter) anchored about 5 cm deep in the rock (Figure 1A). Each sensor installation was protected from water with a plastic sleeve (Figure 1B). We verified that the crumpling of the plastic cover due to wind or other factors do not cause AE. This has been tested during the installation by moving by hand the plastic cover and no AE were generated. Moreover, the windy periods we observed during the experiment have not been recognized to generate AE.

Figure 2 shows an example of AE trace recorded at channel 1, with the trigger level, the maximal and minimal amplitude and the method for calculating the signal energy.

The site shows some heterogeneities in terms of the spatial distribution of fractures (coexistence of compact and fractured zones), microtopography (convex and concave zones) and hydraulic conditions (dry and wet zones). Sensor locations (Figure 1C), referred to as AE1–AE6, have been chosen to investigate different configurations of fractured or compact rock and wet or dry conditions. AE1 is installed in compact and homogeneous rock that is barely fractured in a radius of about one meter. The rock surface bulges out slightly in this area. It has been uncovered from snow one hour before installation, with some snow remaining about 30 cm below the sensor. AE2 has compact, lightly fractured rock that is slightly concave outward and subject to melt water flow from above. AE3 is located in fractured, concave but rather dry rock. AE4 is in fractured rock that is convex and apparently dry in surface. But a gully containing snow is located 0.5 m above it that could supply water in the vicinity. AE5 is installed in compact rock in an overhang underneath a gully and could receive melt water through fractures. AE6 is installed in compact rock in a gully receiving melt water from above. AE5 and AE6 are located near a fracture zone in the deepest

part of the gully; the rock mass to their left is slightly overhanging and may be prone to movement. AE1–AE4 were installed on 6 April, AE5 and AE6 on 7 April 2010. All sensors were uninstalled on 10 April 2010. The Permasense measurement site (Hasler et al., 2008; Beutel et al., 2009) at the same location provides rock temperature data, measured close to sensor AE3, at depths of 10, 35, 60 and 85 cm (Hasler et al., 2011).

3. Results

The system has been operated continuously for four days for AE1–AE4 and three days for AE5–AE6. Air temperatures fluctuated between -2 and -10° C during this time. There were virtually no clouds and radiative diurnal cycles caused near-surface rock temperatures to rise to 10° C during the day and cool to -5° C during nights. Diurnal thawing penetrated about 20 cm deep into the rock wall which remained continuously frozen at greater depths. Due to snowfall in the days before, small snow patches in concave portions of the rock wall locally provided melt water flow during the day. Several thousand events were recorded at each sensor, allowing a robust statistical analysis (Table 1). Because of the large sensor spacing, attenuation precluded the detection of individual events on several sensors. Given the frequency range at which the sensors operate, the detected events can be expected to have their source within the meter scale around the sensor. Since event source localization is impossible, detected events are thus considered to be close to the receiving sensor.

Figure 3 reports the time evolution of AE activity and temperature of the rock at 10, 35 and 60 cm depth as a function of the hour of the day. It highlights the connection between the daily fluctuations of AE activity and that of rock temperature during the monitoring period. For the entire duration of the experiment, the temperature at 35 cm depth remains below 0°C whereas it remains under 0°C at 60 cm depth. The temperature at 10 cm depth exhibits freeze-thaw cycles with temperature ranging from -5°C to 10°C. At this depth, the refreezing can by seen by the plateau characterizing the temperature near

zero in the evening (i.e. at $h \simeq 20$ on days 1–2) when temperature decreases more slowly due to latent heat of water. This time period corresponds to a small peak of the AE activity visible on AE1, AE3, AE5 and AE6. We recall that our analysis is based on a single point measurement of rock temperature. The spatial variability of temperature at different locations could thus partly explain the shift seen in AE activity observed for the different sensors.

The AE activity appears to be significantly larger when the temperature is below zero. The largest AE activity takes place during colder (night-time) periods, when the near-surface of the rock refreezes. This is observed for all the sensors with the notable exception of AE5. Sensors AE1, AE3 and AE5 show activity peaks significantly smaller than AE2, AE4 and AE6. AE1 and AE3 are located in dry areas whereas AE2, and AE6 are located in wet areas with melting water coming from upslope. AE4 was located in an apparently dry area but the presence of snow 0.5 m above could provide melting water that was not visible on the surface. In contrast to the other sites, any meltwater reaching AE5 would have to percolate through fractures. No water comes from the surface due to its situation under an overhang. These observations express the large spatial variability of the near-surface AE activity. They also suggest that the availability of water has a strong control on AE activity. In order to verify the dependence between AE activity and temperature we calculate the distribution of events as a function of the temperature (Fig. 4 left). The relationship between negative temperatures and AE activity appears clearly for all the sensors except AE5. Between 70% and 95% of the events are recorded during negative temperature periods, whereas for AE5, this proportion is only of 37% (see Tab. 1 for details). One may note also that a slight AE peak is visible around temperature zero. The difference in the amplitude of the AE activity between dry and wet areas is confirmed. In order to take into account the fact that much more time is spent in each temperature increment below zero than above, we normalized the event number by the time spent into each temperature interval (Fig. 4 right). the temperature dependence appears stronger for sensors AE2 AE4 and AE6, and weaker for sensors AE1 and AE3. The particularity of

the sensor AE5 appears stronger.

We analyzed the scaling properties of the AE focusing on the domains of energy and time and described other striking behavior of the measured data. For each sensor we calculated the distribution of event energy for the entire duration of the experiments. The PDF's of event energy (Fig. 5) show a power-law (PL) behavior spanning several orders of magnitude with an exponent $b = 1.55 \pm 0.05$. For E smaller than 100, the pdf shows a clear departure from PL trend characterized by a decrease of the slope toward the smallest events. This effect is commonly related to the completeness of the catalog (see e.g. Wiemer and Wyss , 2000). Under this value, due to the signal attenuation, the smallest events are detected only on the vicinity of the sensor and so the sampling of these events is incomplete. On the contrary, above this value there is no statistical sampling bias on the PL trend can be estimated with confidence.

We verified that the completeness and the PL trend remain unchanged when selecting the events recorded during positive or negative temperature periods. We also verified the effect of selecting only events of energy larger than the completeness. The trends observed on Figures 3 and 4 remain the same, in particular with respect to the temperature dependence of AE activity. The only notable effect is the reduction of the amplitude of AE peaks.

As the PL distribution is characteristic of the rupture processes (Alava et al., 2006), the later observation is the first direct evidence published showing that natural thermal cycling and associated freezing/thawing induce near-surface damage in a rock wall.

In order to investigate scaling properties of the temporal distribution of AE events we use the correlation integral (Grassberger and Procaccia, 1983),

$$C(\Delta t) = 2\mathcal{N}(\Delta t)/(N(N-1)) \tag{1}$$

where N is the total number of damage events, $\mathcal{N}(\Delta t)$ is the number of pairs of events separated by a time smaller than Δt. This integral expresses how the events are distributed in time. If the correlation integral exhibits a PL $C(\Delta t) \sim \Delta t^{D_2}$, the population can be considered as a fractal set, i.e. characterized by a

scaling invariance in time domain, with a correlation dimension D_2. A value of D_2 smaller than 1 indicates a time clustering, i.e. the probability of observing an event is larger when a previous one has occurred within a short time. In other words, an event is more likely to occur within a short separating time from the previous one. Departure from power-law trend or slope changes indicate the existence of characteristic time scale limiting the extent of scale invariance.

Figure 6 shows the correlation integrals obtained for each sensor. At small time scales, a first PL trend is identified over two to three orders of magnitude in time, for all sensors except AE5, with a correlation dimension D_2 between 0.75 and 0.9. The value $D_2 < 1$ expresses the temporal clustering of AE events, i.e. the detected events are strongly correlated over this temporal scale range. The extent of the PL trend towards small time scales is limited by the duration of the recording (1 ms) so no event can be detected with a lower separating time. The upper limit of PL extends to about 0.5 s for AE1 and AE4, 1 s for AE2 and AE6, and 5 s for sensor AE3. This mean that the events are strongly correlated in time within this time scale. So this value can be interpreted as the duration of correlated events series that we may consider as sequences of cascading events, i.e. the temporal correlation length, i.e. the duration for which a pair of events is more correlated in time than in a random serie. For larger separating time the correlation integral displays a rather flat shape until recovering a secondary PL trend. In this region, AE4 and AE5 are characterized by a slope $D_2 \simeq 0.9$ indicating a slightly clustered temporal distribution. The duration of the correlated sequences is about 2-3 hours. For AE3 the secondary power-law trend appears of poor quality, with a low D_2 value corresponding to highly clustered events. On the other hand, a clear secondary power law trend of exponent $D_2 \simeq 0.75$ is observed for AE1, AE2 and AE6, a temporal correlation dimension similar to the one observed at smaller time scales. This power law trend extends up to about $\Delta t = 10 - 12$ hours, indicating scaling properties spreading over the duration of the freezing period.

4. Discussion and conclusions

The first striking aspect of the measurements presented is the relationship between negative temperatures and AE activity, suggesting that damage is related to freezing-induced stresses. As ice is a better wave transmitter than liquid water one may ask if this observation could be an artefact induced by the lack of detection instead of a lack of AE at temperatures $> 0°$. In order to verify this, we compare the two sets of events distinguishing positive and negative temperature periods. A first evidence is that the completeness is the same for the two sets (see section 3). This indicates that there is no significant changes in the event detection. As the attenuation is known to affect the frequency content (Hardy, 2003), we analyse the evolution of the mean frequency of the events. Surprisingly, we observed a slight increase of the mean frequency for warmer periods (Fig. 7), particularly for AE2, AE5 and AE6. This could be interpreted as an effect of the thermal dilation of cracks. The rock material in between cracks expands inducing a closure of cracks and then a reduction of the attenuation. The fact that variations of the frequency are limited could be explained by the resonant nature of the sensors we used. The cracks closure can also induce AE, but this has been shown to be limited compared to the crack shearing process (e.g. Moradian et al., 2010). We also examine the relationship between the signal amplitude and duration, considering that a higher attenuation should correspond to a shorter duration for a given amplitude. We observed no (or slight) variations regarding the temperature. Consequently, the increase of AE activity in sub-zero temperatures is unlikely do be an artefact in the AE detection.

We now discuss the different mechanisms that could induce damage through thermal cycling. A possible mechanism for explaining the relationship between AE and temperature is the differential thermal dilation inducing thermal stressing. In the present case, the amplitude of thermal gradients (in space and time) is limited compared to the one needed for inducing damage within intact rock, as observed at the laboratory or estimated analytically considering

thermo-mechanical coupling (e.g. Fredrich and Wong, 1986; Wai et al., 1982). In the case of already damaged or fractured material, it has been shown that daily thermal cycling can induce shearing along existing fractures (Gunzburger et al., 2005) even in absence of freeze-thaw cycles. The most favorable periods are the ones corresponding to high thermal gradient in time ($\delta T/\delta t$) and in space ($\delta T/\delta z$, z representing the depth). Referring to our experiment, this mechanism could induce AE events when the absolute value of the spatial temperature gradient is high, independently of positive or negative temperature. We estimated the temperature gradient in depth as the difference between temperature measured at 10 and 35 cm depth, divided by their separating distance $\delta T/\delta z = (T_{35cm} - T_{10cm})/0.25m$. Figure 8 shows that most of the AE activity occurred when $\delta T/\delta z > 20°C/m$, when the rock 10 cm below the surface is much cooler than 35 cm below.

Thermo-elastic stresses arise when non-uniform (spatial) gradients in temperature develop in elastic materials, which tend to result from rapidly varying temperatures. Note that, somewhat non-intuitively, thermo-elastic stresses would no be expected in unconfined elastic media if the temperature gradient is uniform even if temperatures vary considerably in space. So this mechanism can be evoked only when the temporal gradient is also high.

Figure 8 shows the temperature gradient in time at 10 cm depth. The maximum absolute value of the temporal gradient occurs at approximatively 13 and 18 hours. These two periods corresponds to AE activity peaks visible on Figures 3 and 8, suggesting that AE could be related to fast contraction/dilation of the rock. As the temperature in depth is stable, the temperature gradient is highly correlated with the shallow temperature (Fig. 8). The highest absolute value of the gradient corresponds to the minimum of the shallow temperature. Consequently it is difficult to distinguish between the impacts of the temperature and of the gradient of temperature on the AE activity.

AE activity was shown to be more intense at locations with melt-water, where large bursts of events where recorded during night-time refreezing. This suggests that water freezing plays an important role in the mechanical load-

ing. A possible origin for the damage is the volume expansion of freezing water contained in fractures, that is often evoked for explaining cryo-fracturing. The volume change provokes considerable ice pressure in the fractures that can propagate and release the induced stresses. This could explain the AE activity peak observed when temperature decreases near zero (Fig. 4). Note that the temporal gradient is very small at this time precluding the effect of fast contraction evoked before. When occurring within in a porous medium, the phase change of water spreads over a temperature range that depends on the pore dimension (Coussy, 2005) and not only for $T \approx 0°C$. This could explain why increased AE is sustained across the entire observed range of negative temperatures and not restricted to temperatures near $0°C$.

Another possible mechanism related to ice formation is the cryo-suction or ice segregation (Hallet et al., 1991; Coussy, 2005). Ice in pores or cracks is surrounded by an unfrozen water film due to disjoining (intermolecular) forces. Disjoining forces between the ice and the rock can then cause ice-filled cracks to widen as water is drawn in from the surrounding medium by a free-energy gradient. This phenomenon operates at temperatures below zero in a temperature range depending mostly on the pore size distribution, permeability and fracture mechanical properties of the rock (Hallet et al., 1991). This could explain why AE activity increases for temperatures several degrees below $0°C$. Moreover, one may keep in mind that the surface was probably much cooler than at a depth of 10 cm during the freezing period.

The former mechanism is related to an increase of the ice pressure within fractures. One may reasonably ask if the AE could be induced by the cracking of ice itself instead of the embedding rock. Ice growth is supposed to induce compression stress in the ice and, due to the reaction of the embedding material, tensile stress at the cracks tips. The ice, as rock do, behaves according the Coulomb failure criterion (Weiss and Schulson , 2009). So its strength is larger in compression than in tension. The symmetrical case applies for the rock around the cracks: its strength is smaller in tension than in compression, more over the crack tips acts as a stress concentrator. This suggests that the rupture

is more likely to occur in the rock rather than in the ice. To test this,one may realize waves velocity measurement during periods without ice, to verify that the damage induced in the rock is increasing with time.

Beside the results common to all sensors we also observed differences between sensors. The amplitude of the AE activity seems to depends both on the fracture state and the water availability. The relationship between AE activity and temperature displays also some variations from sensor to sensor. This could be attributed to the fact that we use a single temperature measurement point that we considered as representative of the whole monitoring area. Spatial variability probably exists (cf Gubler et al., 2011) that we were not able to take into account in more detail here. The sensor AE5 behaves differently than others in the sense that the AE crisis occurred during the day whereas the night time was relatively quiet. In contrast to all others, this sensor was sensitive to AE activity associated with fractures supplied with meltwater from above. The AE activity could then be related to water pressure increase in the fractures that has been shown to be able to produce seismicity even with limited water table fluctuations (Guglielmi et al., 2008). Here we based our discussion on qualitative considerations of water availability. For a more quantitative discussion, it is clear that further measurements are necessary, in particular for assessing the amount of liquid water available for the formation of ice, and the water pressure.This could help us to define the respective roles played by thermal dilation, ice formation and cryosuction in the generation of AE. Such measures should be spatially distributed for better understand the spatial heterogeneity of AE activity.

The spatial variability we observed concerning AE activity, and consequently damage, has major consequences on the potential erosion induced by frost-cracking. Considering the frost-cracking as homogeneous and deriving the potential of damage from calculation based on the air temperature only (e.g. Hales and Roering, 2007; Delunel et al., 2010), could lead to poor estimates of weathering. Another important point for the evolution of the morphology in mountain areas is that fractured zones appears more prone to frost-cracking. This en-

hances the localization of damage that tends to concentrate in already damaged zones. As a consequence, the spatial variability of frost-cracking should increase with time.

The second striking aspect is the PL distribution of the AE event energy, which is clearly identified on all sensors with an exponent $b = 1.55 \pm 0.05$ and verified over six orders of magnitude. This scaling relationship is the signature of the rock micro-fracturing activity. Beside the claim of the possible universality of the b-value, this parameter has been proposed to be dependent on various parameters, in particular on the strength heterogeneity of the material, the applied stress and the proximity of failure (see Amitrano , 2012, and references therein for an extended discussion).

The b-value of 1.55 for the energy pdf (corresponding to 0.55 for the cdf), we observed for our data, is in the range expected for rocks experiencing uniaxial or triaxial compression stress state in laboratory experiences (Lockner, 1993) and is very close to that observed prior to the peak load (Amitrano, 2003; Lockner, 1993) and for creep of compression tests after the onset of tertiary creep (Grgic and Amitrano, 2009) and for seismic forerunners recorded in a cliff before its collapse (Amitrano et al., 2005) although the loading mode is very different. This provides an indication that the stress induced by thermal cycling and/or freezing/thawing of water in rock pores and cracks reaches values close to the rock strength. The fact that the b-value is found to be similar for all sensors indicates that strength heterogeneity and stress, which are the two main factors influencing this parameter, are comparable in the different locations we investigated.

The time distribution of AE also reveals power-law distribution, which is a supplementary indication of the complex behavior the frost induced damage and of the presence of strong interaction between damage events. The damage activity appears to be clustered at two different time scales, for $\Delta t < 5 - 10s$ and for $100s < \Delta t < 10h$. This could be interpreted as the effect of two loading mechanisms for which the interaction operates at different time scale. The first could correspond to cascading events related to the elastic redistribution of stress

when damage occurs. The second could be related to the reloading induced by temperature changes and/or water migration that operates at longer time scales.

In order to investigate these questions more precisely, further measurements estimating the source depth of AE events, the evolution of the liquid water content and of the temperature at depth are crucial. Moreover, the mechanisms through which freeze/thaw-induced stresses can occur also need to be better differentiated under in-situ conditions. differentiated under in-situ conditions.

The experiments of Hallet et al. (1991), revealing sustained microfracturing activity throughout a 3-day period during which temperature and temperature gradients were held constant in the sample, demonstrated the ability of ice segregation to fracture rock. However, in the field, such conditions are never achieved and it may be difficult to robustly distinguish the role of volumetric expansion (as water turns into ice) from that of ice segregation. A number of factors such as solutes, pressure, pore size and pore material can depress the freezing point of water contained in rock (Krautblatter et al, 2010) down to several degrees below 0°C. This explains why ice formation in rock, such as in any porous media, is progressive (Coussy and Fen-Chong, 2005) occurring over a whole range of sub-zero temperatures. Volumetric expansion-induced damage could potentially occur over this whole range of temperatures. Using theoretical arguments, Vlahou and Worster (2010) reported that volumetric expansion can only develop significant pressures ($\sim$10MPa) in water saturated confined (spherical) cavities larger than 1cm in diameter of very low permeability ($10^{-15} cm^2$). This prediction basically rules out the role of volumetric expansion on rock fracture, since such conditions are very seldom (if never) achieved in nature. Contrastingly, a different body of work from the cement and concrete research, has shown theoretically that both crystallization and micro-cryosuction mechanisms can induce pressures of several tens of MPa in a single water-saturated, micrometer-size pore embedded in a porous material (Coussy and Fen-Chong, 2005). While the pore structure of rocks certainly does contain such small features (Fredrich et al, 1995), a partial saturation of pore space, which is often achieved in natural conditions, might give a completely different picture.

The results we have reported in this letter show the feasibility of studying rock damage under natural conditions of thermal cycling and freezing using the AE technique. AE activity was shown to significantly increase in sub-zero temperatures, especially in locations of the rock-wall that are prone to receiving melt water, suggesting that freezing-induced stresses contribute to rock damage. The robust PL distribution of AE event in the domains of energy and time distributions, a common observation in rupture processes dynamics, is an indication that damage is acting in such conditions. These results finally suggest that the framework of further modeling studies (theoretical and numerical) should include damage, elastic interaction and poro-mechanics in order to describe freezing-related stresses.

Acknowledgements

The authors are grateful to the referee for its careful review and suggestions that have contributed to widely enhance the manuscript. The research presented was supported though the project PermaSense funded by the Swiss National Foundation (SNF) NCCR MICS as well as the International Foundation High Altitude Research Stations Jungfraujoch and Gornergrat.

References

Alava, M.J., Nukala, P., Zapperi, S., 2006. Statistical models of fracture. Advances in Physics 55, 349.

Amitrano, D., 2003. Brittle-ductile transition and associated seismicity: Experimental and numerical studies and relationship with the b value. J. Geophys. Res. 108.

Amitrano, D., Arattano, M., Chiarle, M., Mortara, G., Occhiena, C., Pirulli, M., Scavia, C., 2010. Microseismic activity analysis for the study of the rupture mechanisms in unstable rock masses. Natural Hazards and Earth System Sciences 10, 831–841.

Amitrano, D., 2012. Variability in the power-law distributions of rupture events. Eur. Phys. J.-Spec. Top. 205(1), 199-215.

Amitrano, D., Grasso, J.R., Senfaute, G., 2005. Seismic precursory patterns before a cliff collapse and critical point phenomena. Geophys. Res. Lett. 32.

Beutel, J., Gruber, S., Hasler, A., Lim, R., Meier, A., Plessl, C., Talzi, I., Thiele, L., Tschudin, C., Woehrle, M., Yuecel, M., 2009. PermaDAQ: A Scientific Instrument for Precision Sensing and Data Recovery in Environmental Extremes. 2009 International Conference on Information Processing in Sensor Networks, Ieee, New York.

Coussy, O., 2005. Poromechanics of freezing materials. Journal of the Mechanics and Physics of Solids 53, 1689–1718.

Coussy, O., Fen-Chong, T., 2005. Crystallization, pore relaxation and microcryosuction in cohesive porous materials. C. R. Mecanique 333, 507–512.

Cox, S.J.D., Meredith, P.G., 1993. Microcrack formation and material softening in rock measured by monitoring acoustic emissions. International Journal of Rock Mechanics and Mining Sciences & Geomechanics Abstracts 30, 11–24.

Delunel, R., van der Beek, P.A., Carcaillet, J., Bourls, D.L., Valla, P.G., 2010. Frost-cracking control on catchment denudation rates: Insights from in situ produced 10Be concentrations in stream sediments (EcrinsPelvoux massif, french western alps). Earth and Planetary Science Letters 293, 72–83.

Fredrich, J.T., Wong, T.f., 1986. Micromechanics of thermally induced cracking in three crustal rocks. Journal of Geophysical Research 91, 12743–12764.

Fredrich, J.T.,Menendez, B., Wong, T.f., 1995. Imaging the Pore Structure of Geomaterials. Science 268, 276-279.

Gaffet, S., Guglielmi, Y., Cappa, F., Pambrun, C., Monfret, T., Amitrano, D., 2010. Use of the simultaneous seismic, gps and meteorological monitoring for

the characterization of a large unstable mountain slope in the southern french alps. Geophysical Journal International 182, 1395–1410.

Grassberger, P., Procaccia, I., 1983. Measuring the strangeness of strange attractors. Physica D 9, 189–208.

Grgic, D., Amitrano, D., 2009. Creep of a porous rock and associated acoustic emission under different hydrous conditions. Journal of Geophysical Research-Solid Earth 114, 19.

Gruber, S., Haeberli, W., 2007. Permafrost in steep bedrock slopes and its temperature-related destabilization following climate change. Journal of Geophysical Research-Earth Surface 112, 10.

Gubler, S., Fiddes, J., Gruber, S., Keller, M., 2011. Scale-dependent measurement and analysis of ground surface temperature variability in alpine terrain. The Cryosphere Discussions 5, 307–338.

Guglielmi, Y., Cappa, F., Amitrano, D., 2008. High-definition analysis of fluid-induced seismicity related to the mesoscale hydromechanical properties of a fault zone. Geophysical Research Letters 35, 6.

Gunzburger, Y., Merrien-Soukatchoff, V., Guglielmi, Y., 2005. Influence of daily surface temperature fluctuations on rock slope stability: case study of the rochers de valabres slope (France). International Journal of Rock Mechanics and Mining Sciences 42, 331–349.

Gutenberg, B., Richter, C., 1954. Seismicity of the Earth and associated phenomenon. Princeton University Press, Princeton.

Hales, T.C., Roering, J.J., 2007. Climatic controls on frost cracking and implications for the evolution of bedrock landscapes. Journal of Geophysical Research 112, 14 PP.

Hallet, B., Walder, J.S., Stubbs, C.W., 1991. Weathering by segregation ice growth in microcracks at sustained sub-zero temperatures: Verification from

509 an experimental study using acoustic emissions. Permafrost and Periglacial
510 Processes 2, 283–300.

511 Hardy, H., 2003. Acoustic emission/microseismic activity - Principles, Tech-
512 niques and Geotechnical Applications. A. A. Balkema, Lisse, Netherlands.

513 Hasler, A., Gruber, S., Haeberli, W., 2011. Temperature variability and thermal
514 offset in steep alpine rock and ice faces. The Cryosphere Discuss. 5, 721–753.

515 Hasler, A., Talzi, I., Beutel, J., Tschudin, C., Gruber, S., 2008. Wireless sensor
516 networks in permafrost research-concept, requirements, implementation and
517 challenges. Proceedings of the 9th International Conference on Permafrost
518 2008, Fairbanks, Alaska, USA.

519 Krautblatter, M., Verleysdonk, S., Flores-Orozco, A., Kemna, A., 2010.
520 Temperature-calibrated imaging of seasonal changes in permafrost rock
521 walls by quantitative electrical resistivity tomography (Zugspitze, Ger-
522 man/Austrian Alps). J. Geophys. Res.- Earth Surface 115, F02003,
523 doi:10.1029/2008JF001209.

524 Lockner, D., 1993. The role of acoustic emission in the study of rock fracture.
525 Int. J. Rock. Mech. Min. Sci. & Geomech. Abstr. 30, 883.

526 Matsuoka, N., Murton, J.B., 2008. Frost weathering: Recent advances and
527 future directions. Permafrost and Periglac. Process. 19, 195–210.

528 Moradian, Z., Ballivy, G., Rivard, P., Gravel, C., Rousseau, B., 2010. Evaluating
529 damage during shear tests of rock joints using acoustic emissions. Interna-
530 tional Journal of Rock Mechanics and Mining Sciences 47, 590–598.

531 Murton, J.B., Peterson, R., Ozouf, J.C., 2006. Bedrock fracture by ice segrega-
532 tion in cold regions. Science 314, 1127–1129.

533 Sethna, J.P., Dahmen, K.A., Myers, C.R., 2001. Crackling noise. Nature 410,
534 242.

Vlahou, I., Worster, M.G., 2010. Ice growth in a spherical cavity of a porous medium. Journal of Glaciology 56, 196.

Wai, R., Lo, K., Rowe, R., 1982. Thermal stress analysis in rocks with nonlinear properties. International Journal of Rock Mechanics and Mining Sciences & Geomechanics Abstracts 19, 211–220.

Weber, S., Gruber, S., Girard, L., 2012. Design of a measurement assembly to study In-Situ rock damage driven by freezing, pp. 1–5.

Wegmann, M., Keusen, H.R., 1998. Recent geophysical investigations at a high alpine permafrost construction site in switzerland, pp. 1119–1123.

Wiemer, S., Wyss, M., 2000. Minimum Magnitude of Completeness in Earthquake Catalogs: Examples from Alaska, the western United States and Japan, Bulletin of the Seismological Society of America. Bulletin of the Seismological Society of America 90(4), 859–869.

Weiss, J., Schulson, E.M., 2009. Coulombic faulting from the grain scale to the geophysical scale: lessons from ice. J. Phys. D-Appl. Phys. 42(21), 214017.

Sensor	AE1	AE2	AE3	AE4	AE5	AE6
Nb. AE events	1.2×10^4	1.5×10^4	0.2×10^4	1.8×10^4	0.3×10^4	1.6×10^4
R	0.80	0.86	0.70	0.94	0.37	0.75
Water supply	Snow cover	From above	Dry	From above	Through fractures	From above
Fractured	No	Slightly	Yes	Yes	Yes	No
Topography	Slightly convex	Slightly concave	Concave	Convex	Concave	Concave

Table 1: Number of AE events recorded and configuration at each sensor location. R is the proportion of events recorded during negative temperature periods.

Figure 1 : Sensor installation at rock surface (A) and weatherproofing (B) shown for AE4. Sensor locations (C) are referred to as AE1-AE6 in the text.

Figure 2 : Example of an acoustic emission trace recorded on channel 1. The dotted lines indicate the trigger above which the trace is recorded. The signal energy, E, is calculated by summing the squared amplitude over the during of the signal. The maximal and minimal amplitude are shown for information.

Figure 3: AE event rates and rock temperature at 10, 35 and 60 cm depth as a function of the time. Time corresponds to the hour in the day.

Figure 4: AE event rates as a function of the temperature at 10 cm depth. Left: Number of events detected in each temperature interval. The bins are $0.5°C$ width. Right: Event number detected in each temperature interval normalized by the time spent in each interval. Sensors 1 3 and 5 (Top), which are in relatively dry sites, have an AE activity smaller than sensors 2 4 and 6. Except sensor 5, they all show a clear dependence on the temperature, with a huge increase of the AE for negative temperatures and reduced activity for positive temperatures. When normalizing by the time spent in each bin (right draft) the temperature dependence appears stronger for sensors AE2 AE4 and AE6, and weaker for sensors AE1 and AE3. The particularity of the sensor AE5 appears stronger.

Figure 5: AE event energy distribution for all channels for the complete experiment. The Power-law trend with $b = 1.55$ is shown as guideline. The completeness energy is also shown to correspond to 100 (Arbitrary unit).

Figure 6: Temporal correlation integral of AE events for all channels. The dashed lines provide guidelines corresponding to exponents $D_2 = 0.75$ and $D_2 = 0.9$.

Figure 7 Mean frequency of the AE event for each sensors. Blue dots correspond to the individual values whereas red crosses give the moving average for 100 successive events and 90% of overlap.

Figure 8: Top: AE activity for all the sensors. Center: In depth gradient of the temperature. Bottom: rate of change temperature. All values are plotted as a function of hours.

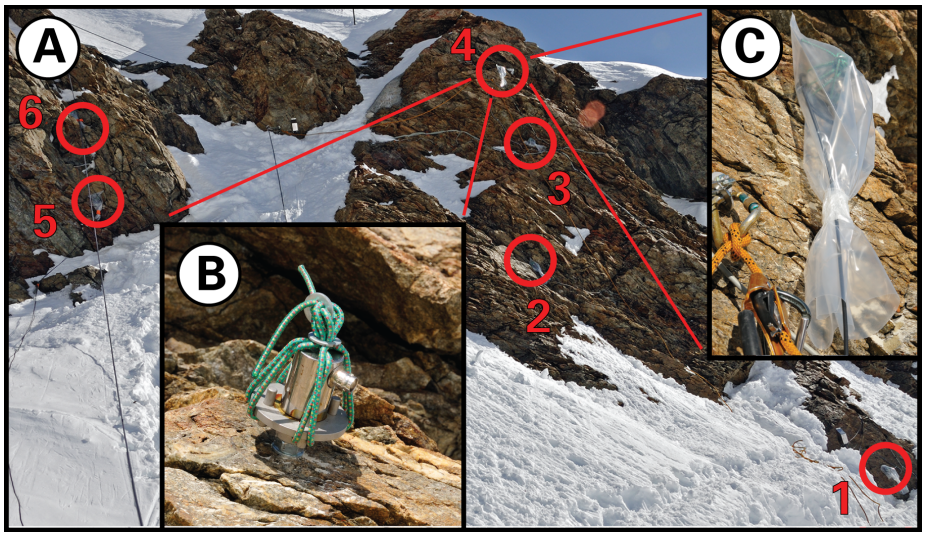

Figure 1: Sensor installation at rock surface (A) and weatherproofing (B) shown for AE4. Sensor locations (C) are referred to as AE1-AE6 in the text.

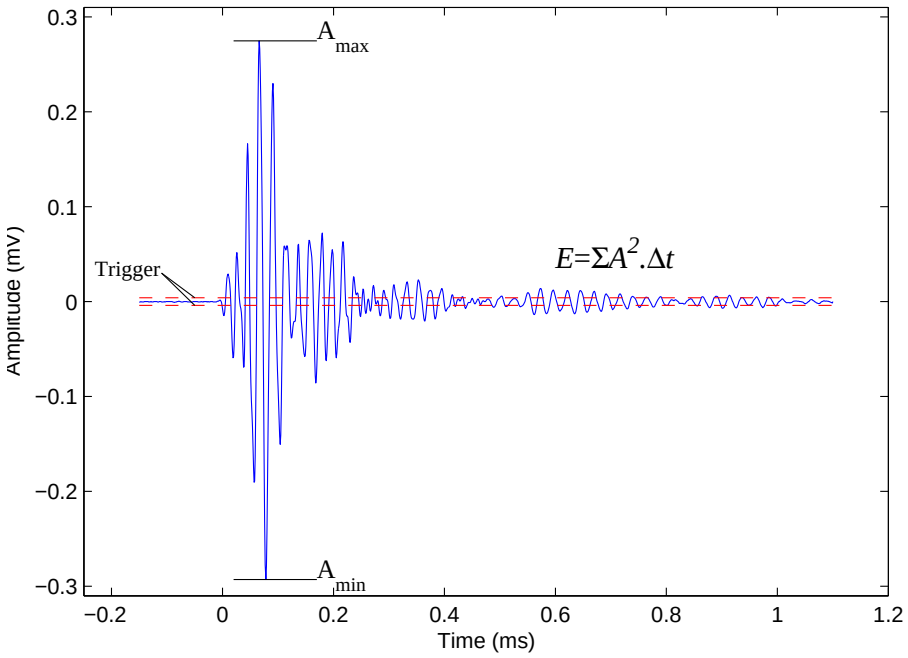

Figure 2: Example of an acoustic emission trace recorded on channel 1. The dotted lines indicate the trigger above which the trace is recorded. The signal energy, E, is calculated by summing the squared amplitude over the during of the signal. The maximal and minimal amplitude are shown for information.

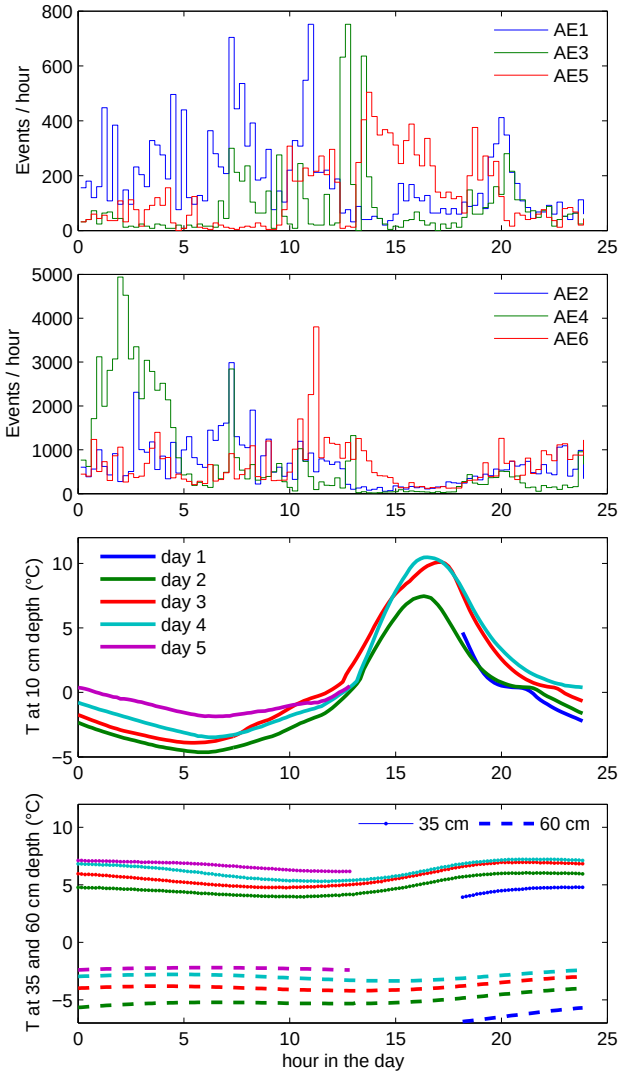

Figure 3: AE event rates and rock temperature at 10, 35 and 60 cm depth as a function of the time. Time corresponds to the hour in the day.

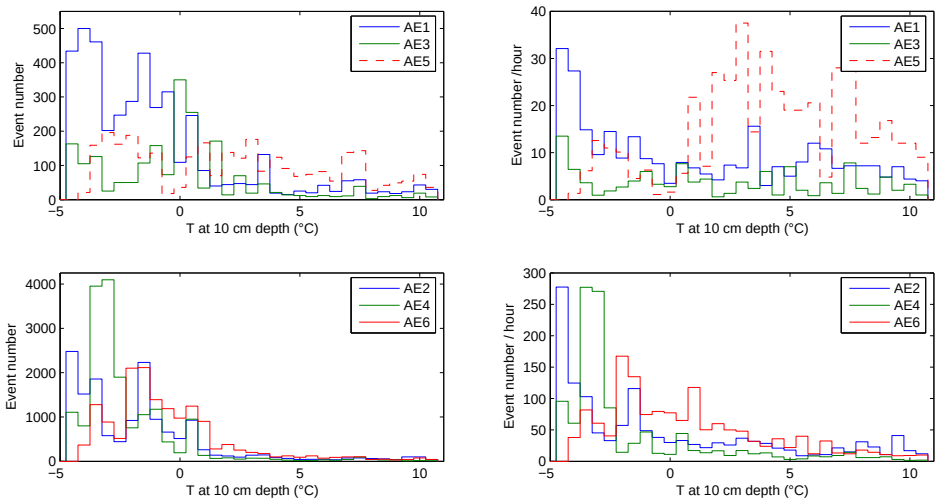

Figure 4: AE event rates as a function of the temperature at 10 cm depth. Left: Number of events detected in each temperature interval. The bins are $0.5°C$ width. Right: Event number detected in each temperature interval normalized by the time spent in each interval. Sensors 1 3 and 5 (Top), which are in relatively dry sites, have an AE activity smaller than sensors 2 4 and 6. Except sensor 5, they all show a clear dependence on the temperature, with a huge increase of the AE for negative temperatures and reduced activity for positive temperatures. When normalizing by the time spent in each bin (right draft) the temperature dependence appears stronger for sensors AE2 AE4 and AE6, and weaker for sensors AE1 and AE3. The particularity of the sensor AE5 appears stronger.

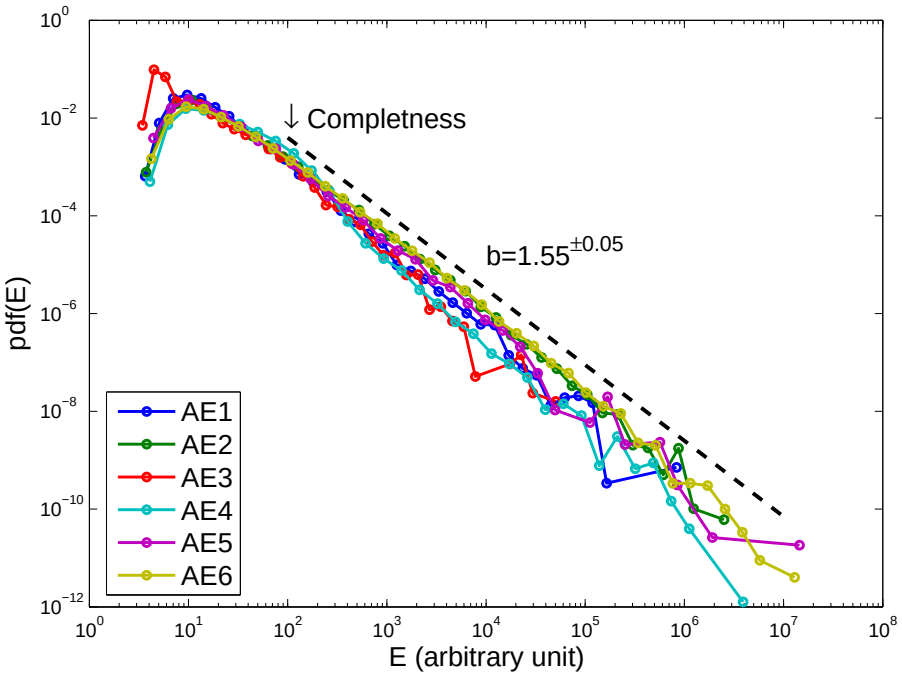

Figure 5: AE event energy distribution for all channels for the complete experiment. The Power-law trend with $b = 1.55$ is shown as guideline. The completeness energy is also shown to correspond to 100 (Arbitrary unit).

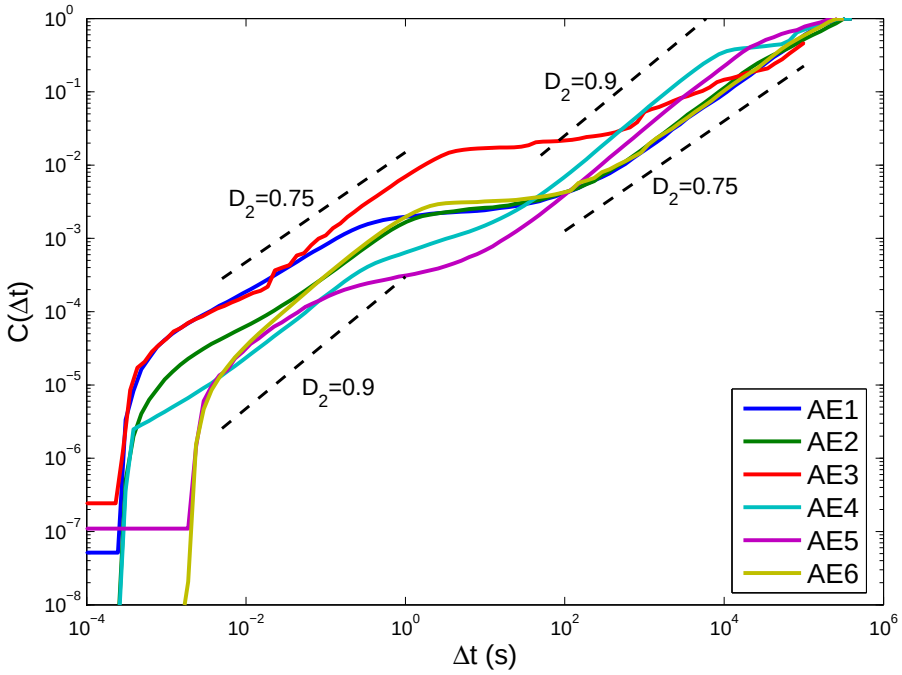

Figure 6: Temporal correlation integral of AE events for all channels. The dashed lines provide guidelines corresponding to exponents $D_2 = 0.75$ and $D_2 = 0.9$.

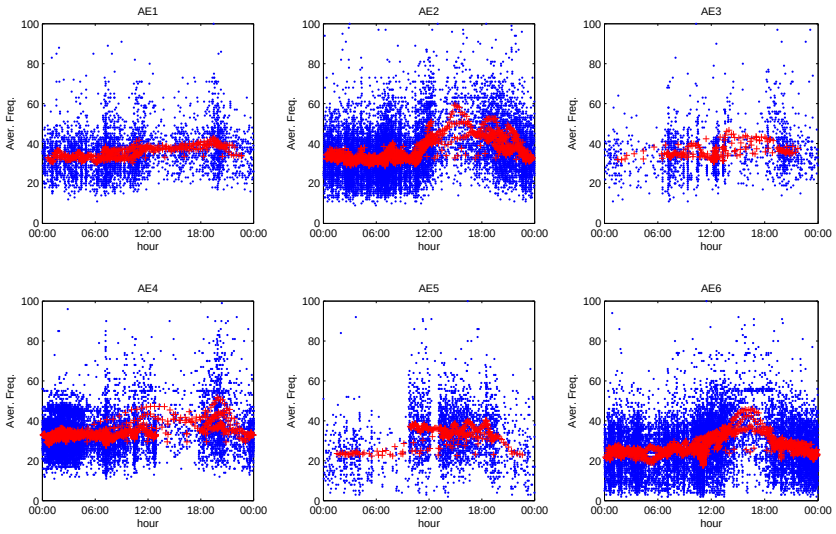

Figure 7: Mean frequency of the AE event for each sensors. Blue dots correspond to the individual values whereas red crosses give the moving average for 100 successive events and 90% of overlap.

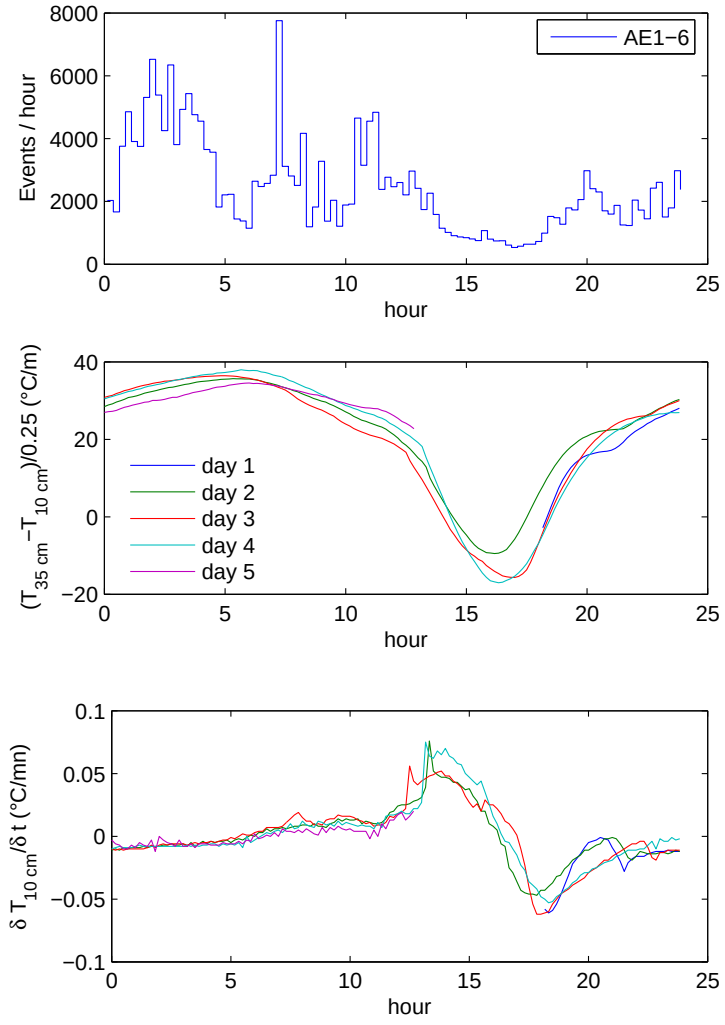

Figure 8: Top: AE activity for all the sensors. Center: In depth gradient of the temperature. Bottom: rate of change temperature. All values are plotted as a function of hours.